

Investigation of electronic, elastic, and optical properties of topological electride Ca_3Pb via first-principles calculations

Chang Sun(孙畅), Xin-Yu Cao(曹新宇), Xi-Hui Wang(王西惠), Xiao-Le Qiu(邱潇乐), Zheng-Hui Fang(方铮辉), Yu-Jie Yuan(袁宇杰), Kai Liu(刘凯), Xiao Zhang(张晓)

Citation: Chin. Phys. B, 2021, 30 (**5**): 057104. DOI: 10.1088/1674-1056/abec38
Journal homepage: http://cpb.iphy.ac.cn; http://iopscience.iop.org/cpb

What follows is a list of articles you may be interested in

Interfacial properties of g-C_3N_4/TiO_2 heterostructures studied by DFT calculations

Chen-Shan Peng(彭春山), Yong-Dong Zhou(周永东), Sui-Shuan Zhang(张虽栓), and Zong-Yan Zhao(赵宗彦)
Chin. Phys. B, 2021, 30 (**1**): 017101. DOI: 10.1088/1674-1056/abb30b

Vanadium based XVO_3 (X=Na, K, Rb) as promising thermoelectric materials: First-principle DFT calculations

N A Noor, Nosheen Mushahid, Aslam Khan, Nessrin A. Kattan, Asif Mahmood, Shahid M. Ramay
Chin. Phys. B, 2020, 29 (**9**): 097101. DOI: 10.1088/1674-1056/ab99ad

Structural evolution and magnetic properties of $ScLi_n$ (n=2-13) clusters: A PSO and DFT investigation

Lu Li(栗潞), Xiu-Hua Cui(崔秀花), Hai-Bin Cao(曹海宾), Yi Jiang(姜轶), Hai-Ming Duan(段海明), Qun Jing(井群), Jing Liu(刘静), Qian Wang(王倩)
Chin. Phys. B, 2020, 29 (**7**): 077101. DOI: 10.1088/1674-1056/ab8d9e

Ab initio study of structural, electronic, thermo-elastic and optical properties of Pt_3Zr intermetallic compound

Wahiba Metiri, Khaled Cheikh
Chin. Phys. B, 2020, 29 (**4**): 047101. DOI: 10.1088/1674-1056/ab7223

A simple rule for finding Dirac cones in bilayered perovskites

Xuejiao Chen(陈雪娇), Lei Liu(刘雷), Dezhen Shen(申德振)
Chin. Phys. B, 2019, 28 (**7**): 077106. DOI: 10.1088/1674-1056/28/7/077106

Investigation of electronic, elastic, and optical properties of topological electride Ca_3Pb via first-principles calculations*

Chang Sun(孙畅)[1], Xin-Yu Cao(曹新宇)[1], Xi-Hui Wang(王西惠)[1], Xiao-Le Qiu(邱潇乐)[2], Zheng-Hui Fang(方铮辉)[1], Yu-Jie Yuan(袁宇杰)[1], Kai Liu(刘凯)[2], and Xiao Zhang(张晓)[1,†]

[1] *State Key Laboratory of Information Photonics and Optical Communications & School of Science, Beijing University of Posts and Telecommunications, Beijing* 100876, *China*

[2] *Department of Physics and Beijing Key Laboratory of Opto-electronic Functional Materials & Micro-nano Devices, Renmin University of China, Beijing* 100872, *China*

(Received 27 January 2021; revised manuscript received 25 February 2021; accepted manuscript online 5 March 2021)

Electrides are unique materials with the anionic electrons confined to the interstitial sites, expecting important applications in various areas. In this work, the electronic structure and detailed physical properties of topological electride Ca_3Pb are studied theoretically. By comparing the crystal structures and band structures of Ca_3Pb and Ca_3PbO, we find that after removing O^{2-} ions from Ca_3PbO, the remaining electrons are confined in the vacancies of the Ca_6 octahedra centers, playing the role as anions and forming an additional energy band compared with that of Ca_3Pb. These interstitial electrons partially result in the low work function of Ca_3Pb. Moreover, the calculated mechanic properties imply that Ca_3Pb has a strong brittleness. In addition, the dielectric functions and optical properties of Ca_3Pb are also analyzed.

Keywords: density functional theory (DFT), density of states (DOS), work function, elastic constant

PACS: 71.15.Mb, 71.20.–b, 73.30.+y, 62.20.dq **DOI:** 10.1088/1674-1056/abec38

1. Introduction

The discovery of novel materials with excellent performance will not only promote the fundamental research in condensed matter physics and material science but also find great value in applications. It is electrides that are one of the paradigms. Electrides represent a special class of compounds whose electrons are partially confined in the structural cavities (e.g., zero-dimensional (0D) cages, one-dimensional (1D) channels, or two-dimensional (2D) interlayer spacings), rather than attached to atoms, and these electrons behave as anions.[1–3] The history of electrides began with the observation of alkali metal ammonia solutions. Later, the organic electride crystal $Cs^+(18C6)_2e^-$ composed of alkali metals and organic components was synthesized.[1] However, the organic electrides are thermally unstable, easy to decompose at room temperature, and sensitive to water and air. In 2003, the first air-stable inorganic electride $[Ca_{24}Al_{28}O_{64}]^{4+}(4e^-)$ (C12A7) was synthesized, making electride materials firmly established in chemistry.[2] Since then, many electrides with various anionic electron confinement topologies have been discovered, such as 0D,[3,4] 1D,[5,6] and 2D electrides.[7,8] Unlike ionic compounds, anionic electrons in electrides are usually loosely bound. Such loosely bound nature of anionic electrons leads to their relatively high mobilities and low work functions, which are key ingredients for various applications, such as electron emitters,[9] anode materials,[10] and high-performance catalysts.[11,12] Especially, the 0D electrides where the anionic electrons reside in the cage space, such as C12A7[2] and LaH_2,[13] have high chemical reactivities and broad applications.[11] Recently, Ca_3Pb was reported to be a 0D electride with a topologically nontrivial band structure.[3] The combination of topological electronic structure and features of anionic electrons in topological electride might lead to exotic physical phenomena, such as floating surface state and the coexistence of 2D surface electride states and topological surface state.[14,15] In order to further understand the physical properties of 0D topological electride Ca_3Pb, in this work, we calculate the electronic structure, work function, mechanical and optical properties of Ca_3Pb in detail. The present work provides theoretical support for experiments and industrial applications.

2. Calculation method

Based on density functional theory (DFT), we performed structural relaxation and electronic structure calculations through the Vienna *ab-initio* simulation software package (VASP).[16] The Perdew–Burke–Ernzerhof generalized gradient approximation was used for the exchange correlation functional.[17] The projector augmented wave (PAW)[18] method was adopted to describe the electron–nuclei interaction. The plane wave cutoff energy was set to 500 eV. A grid of $20 \times 20 \times 20$ mesh k-points was used to sample the Brillouin

*Project supported by the National Natural Science Foundation of China (Grant No. 12074013), the Research Innovation Fund for College Students of Beijing University of Posts and Telecommunications, the Fundamental Research Funds for the Central Universities, China, and the Research Funds of Renmin University of China (Grant No. 20XNH064).

†Corresponding author. E-mail: zhangxiaobupt@bupt.edu.cn

© 2021 Chinese Physical Society and IOP Publishing Ltd

zone. The convergence standards for energy and force were set to 10^{-5} eV and 0.01 eV/Å, respectively. When calculating the mechanical and optical properties, the k-point grid was set to $20\times20\times20$. In the calculation of work functions, the surfaces of (1 0 0), (1 1 0), and (1 1 1) were cleaved and built as slab models. The interplanar spacings of these surface planes are a, $a/\sqrt{2}$, and $a/\sqrt{3}$, respectively. The thickness of the vacuum layer was set to 20 Å to avoid the interaction caused by periodic boundary conditions. The thicknesses of the slabs were set to 3, 5, 7, 9, 11, 13, and 15 atomic layers to study the relationship between the work function and the slab thickness.[19] In the calculation of work function for the Ca-terminated (100) surfaces of Ca_3PbO and Ca_3Pb, the thickness of the slab was set to 15, with the bottom 10 layers fixed and the top 5-layer structure relaxed.[20]

3. Results and discussion

Figures 1(a) and 1(b) show the crystal structures of Ca_3PbO and Ca_3Pb, respectively. Ca_3PbO has an anti-perovskite structure that Pb, Ca and O atoms occupy the corners, face centers and body center of the cubic unit cell, respectively. In addition, the OCa_6 octahedra connect each other by corner sharing. The structure of Ca_3Pb is closely related to that of Ca_3PbO, and the former can be formed by simply removing the O atoms from the latter. Thus, Ca_3Pb also has the cubic symmetry with the space group of $Pm\bar{3}m$ (No. 221), same as Ca_3PbO, and the anionic electrons are trapped at the center of the Ca_6 octahedra.[3] The calculation of lattice relaxation for Ca_3Pb indicates that the optimized lattice constant is 4.950 Å, in good agreement with the experimental result ($a = 4.853$ Å).[21]

Figures 1(c) and 1(d) show the band structures of Ca_3PbO and Ca_3Pb, respectively. Because the Pb element has a large atomic number and the previous study suggests that the spin-orbit coupling (SOC) plays an important role in the transformation of triply degenerate node points near Fermi energy level (E_F) into Dirac points,[3] the SOC is considered during our theoretical calculations in order to describe the band structure of Ca_3PbO and Ca_3Pb properly. It can be clearly seen that for both Ca_3PbO and Ca_3Pb, the bands above E_F (pink color) originate dominantly from the Ca-3d orbitals when the three bands are mainly composed of the Pb-6p orbitals located below E_F (-3.5 eV to E_F, blue color). Moreover, the bands between -8 and -9 eV consist of Pb-6s orbitals. The almost fully occupied Pb-6s and Pb-6p bands suggest that the valence state of Pb atom in both materials can be assigned to -4 approximately. For Ca_3PbO, the three bands derived from O-2p orbitals locate between -5.5 eV and -4 eV, and they are fully occupied, indicating that the valence state of O is -2. Combined with the Ca-4s bands far above E_F, the formula of Ca_3PbO can be expressed as $Ca_3^{2+}Pb^{4-}O^{2-}$.[22] In contrast to Ca_3PbO, once the O atoms locating at the center of OCa_6 octahedra are removed, the three O-2p bands disappear, and importantly, an extra band emerges just below E_F (~ -0.5 eV to 0 eV, red color) in Ca_3Pb. The formation of the extra band strongly suggests that the anionic electrons left in O voids with Ca_6 octahedral coordination form a periodic structure, which is not confined in any cations but stays in the interstitial sites.[3] Moreover, this band is almost completely filled, implying that there should be two electrons in each interstitial site. Thus, the formula of Ca_3Pb can be written as $[Ca_3^{2+}Pb^{4-}]^{2+}\cdot 2e^-$, satisfying the condition of the charge neutrality. It has to be noted that for both Ca_3PbO and Ca_3Pb, there are topological non-trivial band crossing points in the electronic structure. For the former, a 3D gapped Dirac point very close to E_F can be clearly seen at finite momentum along the Γ–X direction, which results from a band inversion of the Ca-$d_{x_2-y_2}$ and Pb-6p bands.[23] For the latter, once the SOC is considered, the triply degenerate node points near E_F along the Γ–X and Γ–R directions are transformed into Dirac points, which are mainly composed of Pb-6p orbitals and interstitial anionic electrons.[3]

The existence of anionic electrons has significant influences on the physical properties of Ca_3Pb. The anionic electrons can lead to a low work function, which is a unique feature of electrides. The work function Φ_{WF} is the minimum energy required to move an electron from the Fermi level to the vacuum.[8] The Φ_{WF} can be calculated by the following formula $\Phi_{WF} = e\Phi_{vac} - E_F$, where Φ_{vac} is the electrostatic potential of the vacuum region and e is an electron charge. The surfaces of Ca_3Pb along (100) and (110) crystal planes have two types of terminations, i.e., CaPb-terminated (100) and (110) surfaces, and Ca-terminated (100) and (110) surfaces. The Φ_{WF}s of Ca_3Pb for different terminations and orientations as a function of slab thickness N (= number of layers) converge quickly when $N \geq 9$. The Φ_{WF}s for $N = 15$ are also listed in Tab. 1. Comparing our present calculated values with and without SOC, the Φ_{WF} of (100) Ca-terminated surface has the smallest value, which is much lower than those values of Φ_{WF}s for other surfaces and even smaller than the Φ_{WF} of Ca (2.9 eV).[20] It could be partially ascribed to the highest density of anionic electrons for the (100) Ca-terminated surface. The relatively loose bound anionic electrons can lead to a low work function. This explains the lower Φ_{WF} of (100) Ca-terminated surface compared with the (110) CaPb-terminated surface because the density of anionic electrons of the former is higher than that of the latter even both surfaces pass through the 1b site (the position anionic electrons occupied). Figure 2 shows the calculated Φ_{WF} of (100) Ca-terminated surface for Ca_3Pb and Ca_3PbO, respectively. When anionic electrons are replaced by O atoms occupying the center of Ca_6 octahedra, the Φ_{WF} of Ca_3PbO increases. This comparison further proves that the relatively loose bound anionic electrons tend to result in a low work function.[7]

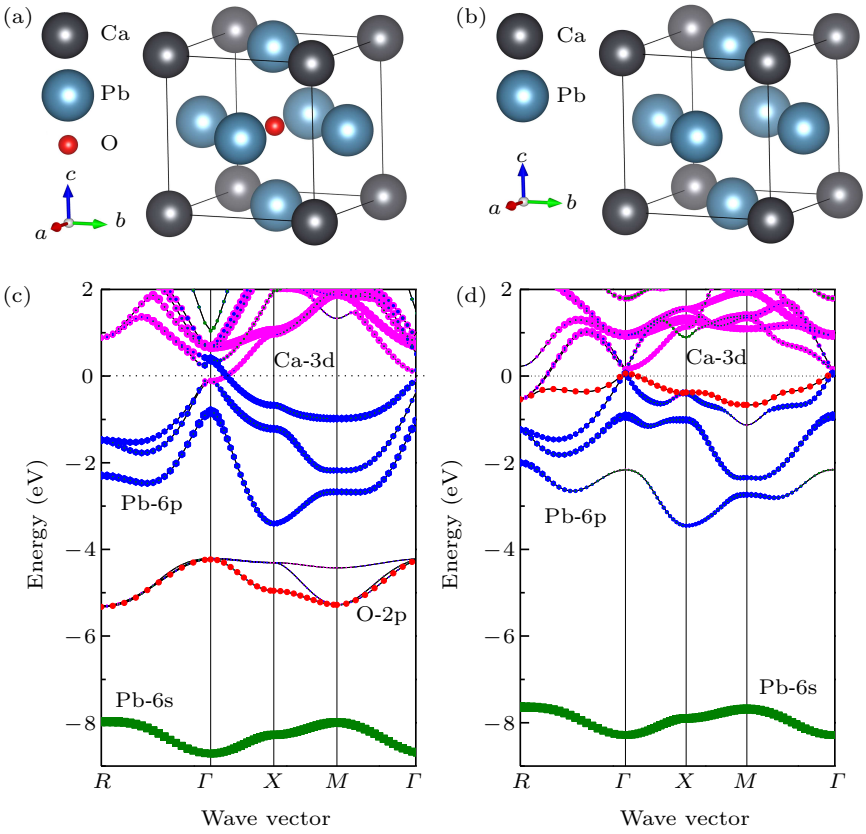


Fig. 1. (a) and (b) Crystal structures of Ca_3PbO and Ca_3Pb, respectively. The blue and gray balls represent Ca and Pb atoms, respectively. The small red ball occupying the body center of the unit cell represents the O atom. (c) and (d) Band structures of Ca_3PbO and Ca_3Pb, respectively. The fat-band representation shows the contributions of atomic orbitals on the projected band structure with Ca-3d orbitals in pink, Pb-6p orbitals in blue, and Pb-6s orbitals in green. The projected band structure from −5 to −4 eV (red color) in panel (c) originates from the O-2p orbitals. In panel (d), the band marked by the red dots is mainly composed of anionic electrons at the interstitial sites.

Table 1. The work function of Ca_3Pb with different surface terminations.

	(100) CaPb-T	(100) Ca-T	(110) CaPb-T	(110) Ca-T	(111)
Φ_{WF} (eV)	3.189	2.763	3.121	2.876	3.078
Φ_{WF} (eV) with SOC	3.097	2.811	3.108	2.838	3.166

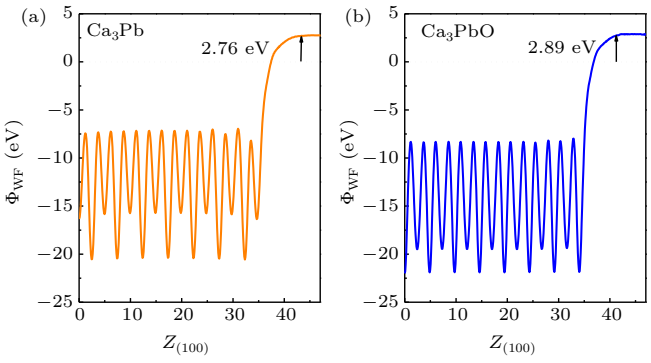


Fig. 2. Work functions for the Ca-terminated (100) surfaces of (a) Ca_3Pb and (b) Ca_3PbO.

The elastic constants characterize the resistance of the material to external stress and deformation. The elastic constants of cubic Ca_3Pb in the linear strain range have only three independent components: C_{11}, C_{12}, and C_{44}, which are 61.89 GPa, 21.32 GPa, and 34.61 GPa, respectively. The elastic properties were calculated by Voigt–Reuss–Hill approximation.[24] Bulk modulus $B = (B_V + B_R)/2$, shear modulus $G = (G_V + G_R)/2$, where

$$B_V = B_R = \frac{(C_{11} + 2C_{12})}{3}, \tag{1}$$

$$G_V = \frac{C_{11} - C_{12} + 3C_{44}}{5}, \tag{2}$$

$$G_R = \frac{5\,(C_{11} - C_{12})\,C_{44}}{4C_{44} + 3\,(C_{11} - C_{12})}. \tag{3}$$

Then, Young's modulus E and Poisson's ratio σ can be obtained by the following formulas:[25]

$$E = \frac{9BG}{3B + G}, \tag{4}$$

$$\sigma = \frac{3B - 2G}{2\,(3B + G)}. \tag{5}$$

The calculated elastic constants satisfy the criterion of crystal structure stability: $C_{11} - C_{12} > 0$, $C_{11} + 2C_{12} > 0$, $C_{44} > 0$.[25] The calculated B, G, E, σ, and B/G are shown in Tab. 2. It can be seen that Ca_3Pb has good mechanical properties and can maintain its stable performance when subjected to mechanical distortion. The result with considering the SOC effect on elastic calculation is also shown. The result with SOC calculation has changed B (4.4%), G (0.9%), E (1.7%), σ (4.9%), and B/G (4.0%) compared with the results without considering SOC, indicating that the effect of

SOC of heavy atom Pb on elastic properties is not obvious. The bulk modulus is an important indicator reflecting the fracture strength, and the shear modulus is an important indicator reflecting the strength against plastic deformation. If the ratio of B to G is less than 1.75, the material is brittle. Otherwise, the material has a better ductility.[26] Different from other typical electrides such as Ca_2N, C12A7 and Y_2C, Ca_3Pb has a strong brittleness.[27–29] The stiffness of the material can be measured by Young's modulus E. The E value of Ca_3Pb is 66.13 GPa, much smaller than these of C12A7 and Y_2C. The ratio of quantities of ionic bonds to covalent bonds in certain material and the ability to resist deformation can be characterized by Poisson's ratio σ. For the materials containing only covalent bonds, the value of σ is less than or equal to 0.1, and for materials that only contain ionic bonds, the value of σ is greater than or equal to 0.25.[30] The σ of Ca_3Pb is 0.184, and it suggests that the chemical bonds in Ca_3Pb are partially covalent, possibly due to the smaller electronegativity difference between Ca and Pb compared with other electrides listed in Tab. 2.

Table 2. Mechanical properties of Ca_3Pb in comparison with other electrides.

Materials	B (GPa)	G (GPa)	E (GPa)	σ	B/G	Ref.
Ca_3Pb	34.82	27.93	66.13	0.184	1.25	this work
Ca_3Pb (with SOC)	33.30	27.67	65.00	0.175	1.20	this work
Ca_2N	35.0	15.0	42.4	0.31	2.33	[27]
Y_2C	68.0	42.0	104.5	0.24	1.62	[28]
C12A7	95.5	47.8	122.9	0.28	2.00	[29]

The degree of elastic anisotropy of a solid can be presented by the elastic anisotropic factor A.[25] It means complete isotropy when the value of A is 1, and anisotropy when A deviates from 1. In the cubic structure, A is given by

$$A=\frac{2C_{44}}{C_{11}-C_{12}}. \tag{6}$$

The calculated A is 1.706, indicating that Ca_3Pb shows a little elastic anisotropy. Three-dimensional surface structures of Young's modulus E and shear modulus G are plotted in Fig. 3. The relationship between E and G and direction can be described by the following formulas:[31]

$$\frac{1}{E}=S_{11}-2\left(S_{11}-S_{12}-\frac{S_{44}}{2}\right)\left(l_1^2l_2^2+l_2^2l_3^2+l_1^2l_3^2\right), \tag{7}$$

$$\frac{1}{G}=S_{44}+4\left(S_{11}-S_{12}-\frac{S_{44}}{2}\right)J, \tag{8}$$

where

$$J=\sin^2\theta\cdot\cos^2\theta+0.125\sin^4\theta\,(1-\cos 4\varphi). \tag{9}$$

Among them, l_1, l_2, and l_3 are the directional cosines in the system, and S_{ij} is the elastic compliance constant. The parameters of θ and φ are Euler angles. The minimum value of E is 50.97 GPa, and the maximum value is 70.80 GPa; the minimum value of G is 20.19 GPa, and the maximum value is 34.61 GPa.

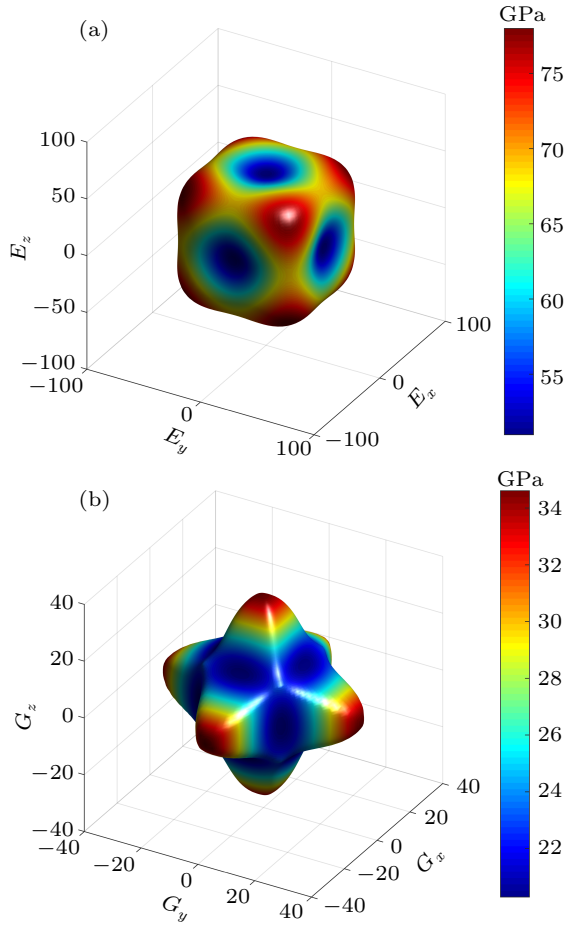


Fig. 3. Three-dimensional surface constructions of (a) Young's modulus E and (b) shear modulus G of Ca_3Pb.

Debye temperature Θ_D is an important parameter in material thermodynamics which is related to specific heat, melting temperature, and lattice vibration. Θ_D can qualitatively reflect the strength of the material's covalent bond. Θ_D can be obtained from the average sound velocity[32]

$$\Theta_D=\frac{h}{k}\left(\frac{3nN_A\rho}{4\pi M}\right)^{\frac{1}{3}}v_m, \tag{10}$$

where h is the Planck constant, k is the Boltzmann constant, n is the number of atoms in the molecule, N_A is the Avogadro constant, M is the molecular mass, and ρ is the density. The average sound velocity v_m can be obtained by the following formula:[32]

$$v_m=\left[\frac{1}{3}\left(\frac{2}{v_t^3}+\frac{1}{v_l^3}\right)\right]^{-\frac{1}{3}}, \tag{11}$$

$$v_l=\left[\frac{\left(B+\frac{4G}{3}\right)}{\rho}\right]^{\frac{1}{2}}, \tag{12}$$

$$v_t=(G/\rho)^{\frac{1}{2}}, \tag{13}$$

where v_l and v_t are the longitudinal and transverse sound velocities, respectively. The calculation results at 0 GPa are shown in Tab. 3. The Θ_D of Ca_3Pb is 262.66 K, which is much smaller than 353 K of Y_2C.[28]

Table 3. Calculated thermodynamic properties of Ca_3Pb at 0 GPa.

property	ρ (g/cm^3)	v_l (m/s)	v_t (m/s)	v_m (m/s)	Θ_D (K)
value	4.48	4010.06	2496.24	271.05	262.66

The optical properties of materials enable us to understand their properties and describe their response to electromagnetic radiation. Since optical properties in the infrared region are usually sensitive to the band structure near the Fermi level, the research on optical properties will provide useful information about the characteristics of electronic structures and inspire their applications in optoelectronic devices. A complex dielectric function $\varepsilon(\omega)$ is the basic data for studying the optical properties, which describes the response of matter to the electromagnetic field. It can be expressed as $\varepsilon(\omega) = \varepsilon_1(\omega) + i\varepsilon_2(\omega)$, where $\varepsilon_1(\omega)$ and $\varepsilon_2(\omega)$ are the real and imaginary parts, respectively. The imaginary part can be obtained by the equation[33]

$$\varepsilon_2(\omega) = \frac{e^2\hbar}{\pi m^2\omega^2}\sum_{v,c}\int_{BZ}|M_{vk}(k)|^2\,\delta\left[\omega_{cv}(k)-\omega\right]\mathrm{d}^3k. \quad (14)$$

The integral covers the first Brillouin zone and the momentum dipole element $M_{vk}(k) = (k\langle u_{ck}|E_{elec}\nabla|u_{vk}\rangle])$ describes the interband transition directly from valence bands to conduction bands, where E_{elec} is the electric field, and the parameters of u_{ck} and u_{vk} are the wave functions of the conduction band and the valence band, respectively. The parameter $h\omega_{cv}(k) = E_{ck} - E_{vk}$ describes the excitation energy required for the interband transition. On the other hand, the real part of the dielectric function about intraband information can be calculated from the imaginary part using Kramers–Kronig transformation[33]

$$\varepsilon_1(\omega) = 1 + \frac{2}{\pi}P\int_0^\infty \frac{\omega'\varepsilon_2(\omega')}{\omega'^2-\omega^2}\,\mathrm{d}\omega', \quad (15)$$

where P is the main value. Figure 4(a) shows the $\varepsilon_1(\omega)$ and $\varepsilon_2(\omega)$ of Ca_3Pb for the energy range up to 50 eV, and Fig. 4(b) depicts the total and partial densities of state (DOS and PDOS). It is obvious that the Fermi surface is dominated by the Pb-6p orbitals with a little contribution from Ca orbitals. Above Fermi energy, the unoccupied orbitals are composed of Ca-3d and Ca-4s orbitals. As shown in Fig. 4(a), the $\varepsilon_2(\omega)$ spectrum has a high absorption below 10 eV and reaches the peak at 2.01 eV in the infrared region, which originates predominantly from the optical transitions of the Pb-6p states to the Ca-3d states. The value of $\varepsilon_2(\omega)$ becomes zero in the range of 12 eV to 23 eV and at the region above 30 eV, suggesting that Ca_3Pb is transparent in these energy ranges. The $\varepsilon_1(\omega)$ spectrum shows that the threshold energy, i.e., the first critical point occurs at 0 eV. From this point, the curve linearly declines to its minimum as the energy increases from 0 eV to 4 eV. This reduction may be due to the intraband transitions, and the large negative values $\varepsilon_1(\omega)$ indicate the metallic nature of this compound. In addition, in the ultraviolet region between 22 eV and 27 eV, Ca_3Pb exhibits some small peaks.

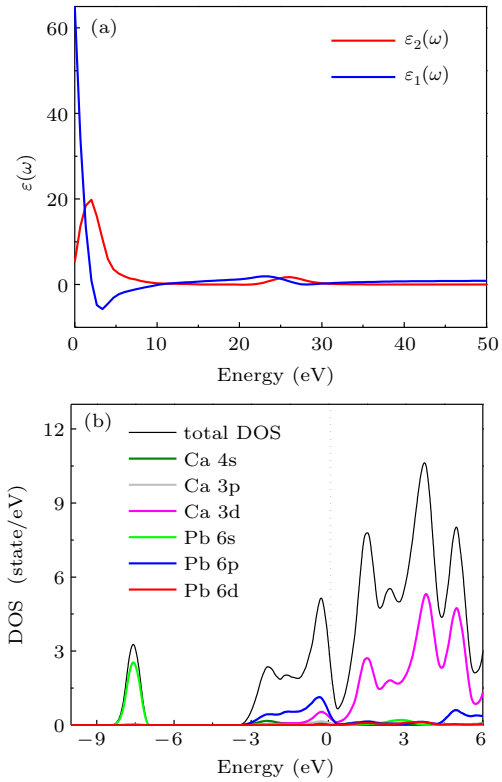


Fig. 4. (a) Dielectric function of Ca_3Pb, in which the red curve is the imaginary part and the blue one is the real part. (b) Total and partial density of states of Ca_3Pb.

Based on the complex dielectric function, we can get some important optical functions, such as absorption coefficient $\alpha(\omega)$, refractive index $n(\omega)$, reflectivity $R(\omega)$, and electron energy loss spectroscopy (EELS, $L(\omega)$).[33]

The calculated results are presented in Fig. 5. As shown in Fig. 5(a), a broadening absorption peak appears in the low energy region from 0 eV–10 eV, corresponding to the low energy peak of $\varepsilon_2(\omega)$. The absorption spectrum is caused by the continuous band transition near the Fermi surface, which indicates the properties of metals. Another absorption peak emerges in the ultraviolet region, corresponding to the small peak in the $\varepsilon_2(\omega)$ spectrum between 22 eV and 32 eV. This may be due to the transition from the deep energy level to the conduction band. Up to 35 eV, the absorption coefficient approaches zero. Figure 5(b) shows the energy dependence of $n(\omega)$. The static refractive index $n(0)$ is 7.1, then it decreases rapidly and has the lowest value at about 10 eV. With the energy increasing further, $n(\omega)$ begins to increase again and reaches a peak value at about 22 eV. Figures 5(c) and 5(d) show the $R(\omega)$ and $L(\omega)$ of Ca_3Pb, respectively. The value

of reflectivity at zero frequency $R(0)$ is 0.67. When the incident electromagnetic energy is less than 8.5 eV, the reflectivity oscillates around 0.5. With the increase of incident electromagnetic energy to more than 8.5 eV, the reflectivity decreases sharply. This may be related to the switch of intraband to interband absorptions. The EELS is used to describe the energy loss of an electron passing through a solid at a certain speed. The characteristic peaks of $L(\omega)$ are related to the oscillation of the plasma. The energy loss is the largest at 10 eV (Fig. 5(d)), corresponding to the sharp drop in the $R(\omega)$ when the energy is larger than 8.5 eV and the zero crossing of $\varepsilon_1(\omega)$.

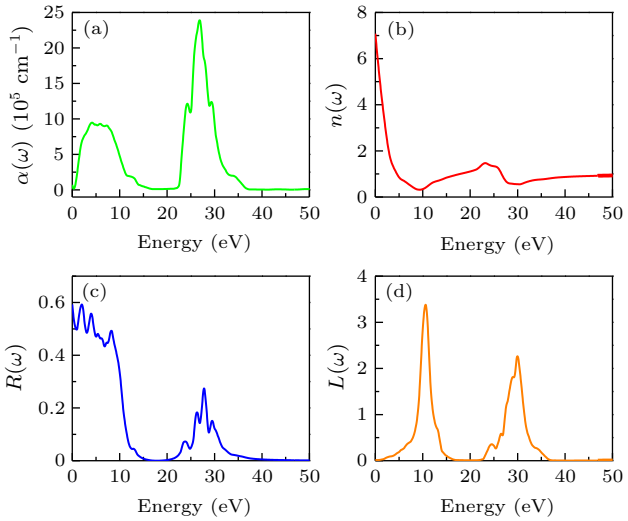


Fig. 5. The energy dependence of (a) absorption coefficient, (b) refractive index, (c) reflectivity, and (d) electron energy loss spectroscopy of Ca_3Pb.

4. Conclusion

We have studied the electronic structure, work function, elastic and optical properties of 0D electride Ca_3Pb based on first-principles calculations. It is found that the interstitial electrons in the center of the Ca_6 octahedron in Ca_3Pb form an additional energy band near the E_F, and the chemical formula of Ca_3Pb can be expressed as $[Ca_3^{2+}Pb^{4-}]^{2+}\cdot 2e^-$. Moreover, the Φ_{WF} of Ca-terminated (100) surface has the lowest work function (2.76 eV) when compared with other surfaces, and it increases when the O atoms replace the anionic electrons, which proves that the characteristic of the low work function of Ca_3Pb partially comes from the loosely bound anionic electrons. The calculations of elastic properties indicate that Ca_3Pb has a strong brittleness. The results of the calculated dielectric function and optical properties show that the peak of the imaginary part of the dielectric function comes from the transition from the Pb-6p band to the Ca-3d band. The present study will deepen the understanding of 0D electride Ca_3Pb and provide theoretical guidance for the potential applications of this material.

References

[1] Ellaboudy A, Dye J L and Smith P B 1983 *J. Am. Chem. Soc.* **105** 6490
[2] Matsuishi S, Toda Y, Miyakawa M, Hayashi K, Kamiya T, Hirano M, Tanaka I and Hosono H 2003 *Science* **301** 626
[3] Zhang X M, Guo R K, Jin L, Dai X F and Liu G D 2018 *J. Mater. Chem. C* **6** 575
[4] Ma Y M, Eremets M, Oganov A R, Xie Y, Trojan I, Medvedev S, Lyakhov A O, Valle M and Prakapenka V 2009 *Nature* **458** 182
[5] Lu Y F, Li J, Tada T, Toda Y, Ueda S, Yokoyama T, Kitano M and Hosono H 2016 *J. Am. Chem. Soc.* **138** 3970
[6] Wan B, Lu Y F, Xiao Z W, Muraba Y, Kim J, Huang D, Wu L, Gou H, Zhang J, Gao F, Mao H K and Hosono H 2018 *NPJ Comput. Mater.* **4** 77
[7] Lee K, Kim S W, Toda Y, Matsuishi S and Hosono H 2013 *Nature* **494** 336
[8] Zhang X, Xiao Z W, Lei H C, Toda Y, Matsuishi S, Kamiya T, Ueda S and Hosono H 2014 *Chem. Mater.* **26** 6638
[9] Hosono H, Kim J, Toda Y, Kamiya T and Watanabe S 2017 *Proc. Natl. Acad. Sci. USA* **114** 233
[10] Hu J P, Xu B, Yang S Y, Guan S, Ouyang C Y and Yao Y G 2015 *ACS Appl. Mater. Interfaces* **7** 24016
[11] Kanbara S, Kitano M, Inoue Y, Yokoyama T, Hara M and Hosono H 2015 *J. Am. Chem. Soc.* **137** 14517
[12] Kuganathan N, Hosono H, Shluger A L and Sushko P V 2014 *J. Am. Chem. Soc.* **136** 2216
[13] Mizoguchi H, Okunaka M, Kitano M, Matsuishi S, Yokoyama T and Hosono H 2016 *Inorg. Chem.* **55** 8833
[14] Hirayama M, Matsuishi S, Hosono H and Murakami S 2018 *Phys. Rev. X* **8** 031067
[15] Huang H Q, Jin K H, Zhang S H and Liu F 2018 *Nano Lett.* **18** 1972
[16] Kresse G and Furthmüller J 1996 *Comput. Mater. Sci.* **6** 15
[17] Perdew J P, Burke K and Ernzerhof M 1996 *Phys. Rev. Lett.* **77** 3865
[18] Blöchl P E 1994 *Phys. Rev. B* **50** 17953
[19] Lu C L, Zhang L, Zhang Y W, Liu S Y and Mei Y 2015 *Chin. Phys. B* **24** 017501
[20] Singh-Miller N E and Marzari N 2009 *Phys. Rev. B* **80** 235407
[21] Helleis O, Kandler H, Leicht E, Quiring W and Woelfel E 1963 *Z. Anorg. Allg. Chem.* **320** 86
[22] Obata Y, Yukawa R, Horiba K, Kumigashira H, Toda Y, Matsuishi S and Hosono H 2017 *Phys. Rev. B* **96** 155109
[23] Kariyado T and Ogata M 2012 *J. Phys. Soc. Jpn.* **81** 064701
[24] Hill R 1952 *Proc. Phys. Soc. A* **65** 349
[25] Metiri W and Cheikh K 2020 *Chin. Phys. B* **29** 047101
[26] Pugh S F 1954 *Lond. Edinb. Dubl. Phil. Mag.* **45** 823
[27] Gaillac R, Pullumbi P and Coudert F 2016 *J. Phys. Condens. Matter* **28** 275201
[28] He Y M 2016 *J. Alloys Compd.* **654** 180
[29] Hussain A, Mehmood S, Rasool M N, Aryal S, Rulis P and Ching W Y 2016 *Indian J. Phys. Proc. Indian Assoc. Cultiv. Sci.* **90** 917
[30] Bannikov V V, Shein I R and Ivanovskii A L 2007 *Phys. Status Solidi Rapid Res. Lett.* **1** 89
[31] Wu Q and Li S 2012 *Comput. Mater. Sci.* **53** 436
[32] Anderson O L 1963 *J. Phys. Chem. Solids* **24** 909
[33] Yang Z J, Guo Y D, Li J, Liu J C, Dai W, Cheng X L and Yang X D 2010 *Chin. Phys. B* **19** 077102